Langmuir

Article

pubs.acs.org/Langmuir

Structure of [C_4mpyr][NTf_2] Room-Temperature Ionic Liquid at Charged Gold Interfaces

Yansen Lauw,[†,∥] Michael D. Horne,[†] Theo Rodopoulos,[†] Vera Lockett,[‡] Bulent Akgun,[§,⊥] William A. Hamilton,[∥] and Andrew R. J. Nelson[∥,*]

[†]CSIRO Process Science and Engineering, Bayview Avenue, Clayton South, Victoria 3169, Australia

[‡]Ian Wark Research Institute, University of South Australia, Mawson Lakes, 45 SA 5095, Australia

[§]Center for Neutron Research, National Institute of Standards and Technology, Gaithersburg, Maryland 20899, United States

[⊥]Department of Materials Science and Engineering, University of Maryland, 48 College Park, Maryland 20742, United States

[∥]Australian Nuclear Science and Technology Organisation, Locked Bag 2001, Kirrawee DC, NSW 2232, Australia

Supporting Information

ABSTRACT: The structure of 1-butyl-1-methylpyrrolidinium bis(trifluoromethylsulfonyl)imide ([C_4mpyr][NTf_2]) room-temperature ionic liquid at an electrified gold interface was studied using neutron reflectometry, cyclic voltammetry, and differential capacitance measurements. Subtle differences were observed between the reflectivity data collected on a gold electrode at three different applied potentials. Detailed analysis of the fitted reflectivity data reveals an excess of [C_4mpyr]$^+$ at the interface, with the amount decreasing at increasingly positive potentials. A cation rich interface was found even at a positively charged electrode, which indicates a nonelectrostatic (specific) adsorption of [C_4mpyr]$^+$ onto the gold electrode.

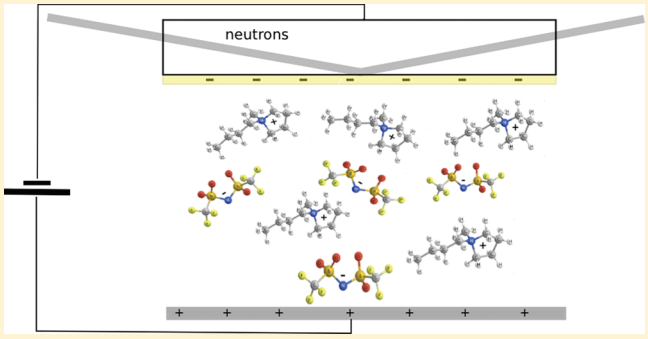

INTRODUCTION

Room-temperature ionic liquids (RTILs) have attracted an enormous amount of interest in the last few decades due to their favorable physicochemical properties, such as low melting point, good thermal stability, and low volatility.[1−5] These properties make them attractive potential solvents for many industrial applications, such as energy storage and metals production.[6−13] Some ILs are particularly resistant to oxidation and reduction and have electrochemical windows up to 6 V making them especially suited as solvents for the electrodeposition of reactive metals such as aluminum. For example, in the current method for aluminum production the metal is electrodeposited from a molten salt at temperatures up to 1000 °C.[14,15] There is significant interest in developing new methods for bulk and high-purity aluminum which avoid the difficulties of the high-temperature process, such as high energy demand and hazardous emissions. RTILs are one of the novel technologies being investigated for this purpose.

The morphology of a metal electrodeposit is influenced by a number of factors besides the coordination environment of the dissolved metal ion. These factors include the viscosity and Lewis acidity of the solvent, the temperature, the duration of the deposition, the applied electrode potential, and the electrical double-layer (EDL) structure at the liquid-electrode interface.[6−13,16,17] Studies of the EDL structure in RTILs at uncharged solid−liquid interfaces and gas−liquid surfaces have been reported in the literature. These studies made use of surface forces apparatus, atomic force microscopy (AFM), surface tunneling microscopy (STM), and X-ray and neutron reflectometry techniques.[18−26] The results showed that strong interplay between electrostatic interaction and steric hindrance in RTILs causes the formation of alternating layers of cations and anions at interfaces. Such alternating layers are typically only a few nanometers thick and thus can generate a large electrostatic potential field of up to ∼10^9 V/m. The thickness and polarity of each alternate layer will affect the value of the EDL capacitance and may also affect the rate of electron transfer.[27−37] Higher capacitance values are obtained when the polarization of ions in the EDL increases, the thickness of the EDL decreases, or both.

Experimental studies of the EDL structure in RTILs as a function of applied electrode potential are rare, although indirect studies of ion adsorption at aluminum surfaces have been reported by Endres et. al.[9,38] These studies concluded that at the negative potentials required to enable aluminum to be electrodeposited the cation of the ionic liquid is adsorbed preferentially at the interface and modifies the deposit morphology.

Recent efforts in probing the potential-dependent EDL structure in RTILs have mainly focused on the first

Received: February 8, 2012
Revised: April 13, 2012
Published: April 19, 2012

(Helmholtz) layer of EDL in imidazolium-based RTILs.[39−42] The results indicate that the cation in the Helmholtz layer is oriented parallel to the surface at negative applied potentials. This orientation shifts toward the normal angle with increasingly positive potentials. To gain more insights on changes in the overall EDL structure as a function of applied potential, we performed neutron reflectometry (NR) studies at an electrified Au-RTIL interface. Results from the NR measurements were then analyzed with the help of the complementary cyclic voltammetric and differential capacitance data. In this study 1-butyl-1-methylpyrrolidinium bis-(trifluoromethylsulfonyl)imide ([C_4mpyr][NTf_2]) was used as a model RTIL. It is one of the most common and best understood RTILs with favorable physicochemical properties for electrochemical applications, such as low viscosity, low melting point, high conductivity, and high electrochemical stability.[43] The molecular structure and size of [C_4mpyr][NTf_2] is shown in Figure 1.

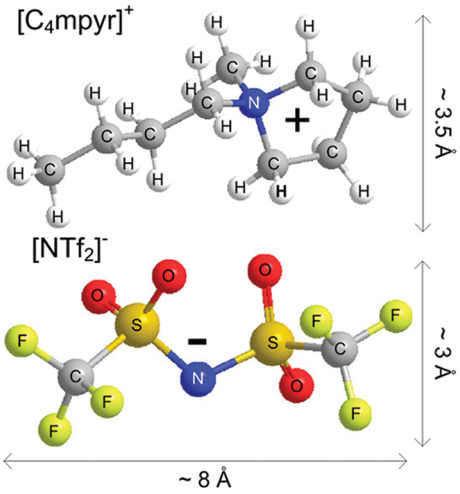

Figure 1. Molecular structure of [C_4mpyr]$^+$ and [NTf_2]$^-$.

NR is a particularly useful technique to use for interfacial studies of these materials because measurements can be made in a completely closed cell, allowing the interface to be probed while maintaining a rigorously clean environment.[44]

■ EXPERIMENTAL SECTION

The schematic of the electrochemical cell used in this study can be found in Lauw.[45] The cell comprises three electrodes: a 10 cm-diameter working electrode coated with a gold film and a glass disk coated with fluorine-doped tin oxide as a counter electrode. Here we measured the Au thickness to be 264 Å with a roughness of 10 Å. Previous X-ray reflectometry measurements on the same film indicated a smaller roughness,[45] 5.4 Å. Such discrepancies can occur because the sampling area of the two techniques are quite different, which magnifies the effect of small changes in film properties across the wafer.

The two electrodes are separated from each other by a thin fluoropolymer gasket which defines the cell reservoir. A silver wire acts as a pseudoreference electrode. The gold film was deposited onto a polished silicon wafer precoated with an adhesive Cr-layer using vacuum thermal evaporation. The gold and chromium films were characterized by X-ray reflectometry and X-ray diffraction as described in a previous work.[45] The film was found to be polymorphous with the Au(111) crystal phase predominant. Prior to placing the electrodes in the cell, the gold and glass electrodes were cleaned using HPLC-grade isopropanol. The gold electrode was subsequently cleaned with ozone for 5 min.[46] During data collection, the applied electrode potential was regulated using an eDAQ EA161 potentiostat (the maximum current density was less than 4 μA/cm^2 at all times). A full description of the electrochemical cell and the components which comprise it can be found in Lauw et al.[45]

The ultrahigh purity [C_4mpyr][NTf_2],[47] obtained from Merck has the following physical properties: melting point −18 °C, viscosity at 25 °C 85 × 10^{-3} Pa·s, conductivity at 25 °C 2.2 × 10^{-3} S·cm^{-1}, dielectric constant 11.9. Karl Fischer analysis showed it contained 41 ppm water. The neutron scattering length density (SLD) of [C_4mpyr][NTf_2] was calculated based on its mass density (Anton Paar Densitometer DMA5000) at 25 °C, which is 1.3945 g/cm^3 (the corresponding molecular volume is 503 Å^3). The SLDs for each component were calculated by summing the bound coherent scattering lengths[48] of the consituent atoms and dividing by the molecular volume. The scattering length density of a material indicates how strongly a neutron interacts with it. The literature[49,50] indicates that the molecular volumes of [C_4mpyr]$^+$ and [NTf_2]$^-$ are 253 and 230 Å^3 respectively. However the sum total of these volumes (483 Å^3) is 1.041 times less than the measured value of 503 Å^3. Therefore, the molecular volumes used to calculate the SLD were multiplied by this number: [C_4mpyr]$^+$ = 263.4 Å^3 and [NTf_2]$^-$ = 239.6 Å^3. The SLDs for [C_4mpyr][NTf_2], its constituent ions, and all the components of the working electrode, are shown in Table 1.

Table 1. Neutron SLD of [C_4mpyr][NTf2], Its Constituent Ions, and the Working Electrode Components

species	SLD/10^{-6} Å^{-2}
[C_4mpyr][NTf_2]	1.59
[C_4mpyr]$^+$	−0.21
[NTf_2]$^-$	3.57
Au	4.50
Cr	3.03
SiO_2	3.47
Si	2.07

■ NEUTRON REFLECTOMETRY

A series of NR measurements were conducted at ANSTO's OPAL reactor using the time-of-flight (energy dispersive) Platypus instrument.[51,52] The range of momentum transfer was $0.005 < Q/\text{Å}^{-1} < 0.15$, with Q being equal to $[4\pi.\sin(\theta)]/\lambda$, where θ and λ are the angle of incidence and wavelength of the neutron, respectively. The fractional Q-resolution of the measurement ($\Delta Q/Q$) was 4%. Before exposing the gold film to the RTIL neutron and X-ray reflectivity patterns from the gold electrode against air were measured and analyzed to obtain the thickness and roughness of the Au, Cr, and native SiO_2 layers of the working electrode. The Au-RTIL interface was probed by directing the neutron beam through the silicon and reflecting from the electrode-RTIL interface. The NR data were collected at room temperature for three distinct applied potentials against a silver wire pseudoreference electrode: −1000 mV, open circuit potential (−300 mV) and at +1500 mV. These potential values were then rescaled with respect to Ag|Ag$^+$ (10 mM Ag triflate [OTf] in [C_4mpyr][NTf_2]), which is the reference electrode used in the differential capacitance measurement. The potential of the silver wire pseudoreference electrode was measured as +245 ± 13 mV vs Fc|Fc$^+$ (five repetitions), and the potential calibration from Fc|Fc$^+$ to Ag|Ag$^+$ yields +350 ± 5 mV (five repetitions). The three applied potentials are thus −1595, −895, and +905 mV vs Ag|Ag$^+$ reference electrode. They are located within the electrochemical window (between the cathodic and anodic limits) of

$[C_4mpyr][NTf_2]$ on a gold electrode, as shown by the cyclic voltammogram in Figure 2a. The potential values are marked as

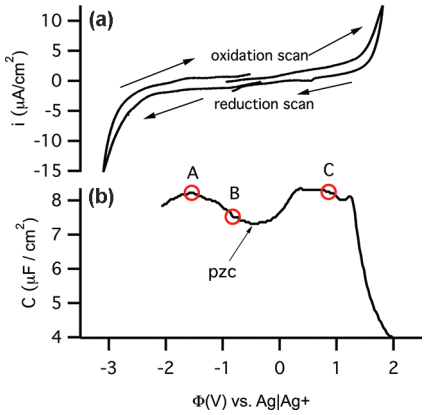

Figure 2. (a) Cyclic voltammogram of ultrahigh purity $[C_4mpyr]$-[NTf2] on a gold electrode, recorded at a scan rate of 20 mV/s. (b) Corresponding differential capacitance curve obtained from impedance measurements.[53] The NR data were collected at three potential values, i.e., at −1595, −895, and +905 mV vs Ag|Ag^+, which are indicated by points A, B, and C, respectively.

points A, B, and C on the differential capacitance curve in Figure 2b. The reproducibility of the experiment was confirmed by a series of repeated NR measurements using different gold electrodes, with the potentials applied in the reverse order.

MODELING

Each measured NR data set was analyzed by creating a model of the scattering length density profile perpendicular to the Au/bulk IL interface.

(i) Part of the Au-layer, the interface, and a proportion of the bulk liquid are divided into 200 sublayers;

(ii) The volume fraction of Au, $[C_4mpyr]^+$, and $[NTf_2]^-$ in each sublayer are assigned under incompressibility (space filling) constraints. The volume fraction of Au is described by a Heaviside (step) function, i.e., equal to unity if the sublayer is located within the Au-layer and zero otherwise. Accordingly, the volume fraction of ions for any sublayer located within the Au-layer is equal to zero. For sublayers situated beyond the Au-layer, the local volume fraction of $[C_4mpyr]^+$ and $[NTf_2]^-$ is calculated from the mole fraction profile of the cation $x_{[C_4mpyr]+}(z)$, where z is the distance from the Au/bulk IL interface:

$$x_{[C_4mpyr]^+}(z < 0) = 0$$

$$x_{[C_4mpyr]^+}(0 < z < t) = F$$

$$x_{[C_4mpyr]^+}(t < z) = \left(F - \frac{1}{2}\right)\cos\left[\frac{2\pi(z-t)}{\lambda}\right] \exp\left[-\frac{z-t}{l}\right] + \frac{1}{2} \quad (1)$$

t is the thickness of a layer adjacent to the Au interface with uniform mole fraction, F, of cation ($0 < F < 1$). Next to this is an exponentially damped cosine function (decay length, l and wavelength λ), used to represent the expected oscillatory layering of cations and anions at the electrode-RTIL interface. Space filling constraints mean that $x_{[NTf2]^-}(z > 0) = 1 - x_{[C_4mpyr]^+}(z > 0)$.

(i) A normalized Gaussian function is created, with its mean value located at the electrode-RTIL phase boundary and its standard deviation equal to the roughness of the Au-layer. This Gaussian function is then convolved with the volume fraction profile of each component. The convolved volume fraction profiles are used to generate the SLD profile across the interface and the corresponding NR curve.

(ii) The model parameters described by eq 1 are then adjusted to minimize the least-squares difference (χ^2) between this theoretical curve and the measured NR data. We use a genetic optimization technique, with error weighting and resolution smearing, in the MOTOFIT[54] program. Uncertainties in parameters were obtained via Monte Carlo resampling. The computer code required to carry out this fit is available in the Supporting Information.

We use the slicing method described above for two reasons. First, the function we are trying to describe in eq 1 is smoothly varying. Using a multitude of slices approximates the function well, but the same cannot be said for a model only possessing one or two layers (slices) that have a uniform SLD. Second, the slicing approach is also required because the thickness of the adsorbed cation/anion layer is the same order of magnitude as the roughness of the Au film. In this regime, the Nevot and Croce[55] approach for treating roughness loses its validity. However, the slicing and convolution approach we use here is rigorous and still applicable. At small roughness values the Nevot−Croce approach and the slicing approaches are equivalent.

CYCLIC VOLTAMMETRY AND DIFFERENTIAL CAPACITANCE

Cyclic voltammetry measurements of ultrahigh purity $[C_4mpyr][NTf_2]$ were conducted under an inert argon atmosphere on a gold electrode (1 mm in diameter) using a potential scan rate of 20 mV/s. A silver wire was used as a pseudoreference electrode and the results were rescaled against a Ag|Ag^+ reference electrode so that they could be directly compared with the differential capacitance measurements. The cyclic voltammogram shown in Figure 2a is constructed from two separate scans, one toward the cathodic and one toward the anodic limit of $[C_4mpyr][NTf_2]$. These scans were performed separately to prevent decomposition products formed at one potential limit, (such as the reduction of $[C_4mpyr]^+$ and/or $[NTf_2]^-$ at negative potentials) interfering with the determination of the other potential limit.[56,57]

The differential capacitance curve of a gold electrode (1 mm in diameter) in $[C_4mpyr][NTf_2]$ is shown in Figure 2b. The differential capacitance was calculated from impedance measurements recorded using a Zahner IM6-ex electrochemical workstation. The RTIL was held at room temperature and under high vacuum (10^{-5} Torr), with a Ag|Ag^+ (10 mM Ag[OTf], $[C_4mpyr][NTf_2]$) reference electrode and a large area platinum counter electrode. The differential capacitance was measured every 0.03 mV using a 1 kHz perturbation and an acquisition time of 100 s. The accuracy of the measurements was checked at several potentials using full impedance fitting in the frequency range 50−7000 Hz. The equivalent circuit used

for fitting consists of an electrolyte resistance and constant phase element with an exponent of 0.87. Full details of the equipment and methods used for the differential capacitance measurements are described fully in our earlier publication.[36]

RESULTS AND DISCUSSION

The differential capacitance curve in Figure 2b has a camel shape with one local minimum and two maxima. The camel-shaped capacitance curve for RTILs has been theoretically predicted and widely discussed in the literature.[27−37] In our recent modeling publication, we showed that such a capacitance curve can result from relatively large ion sizes and non-homogeneous ion polarizations at the interface.[37] The local minimum of the capacitance curve is typically regarded as the point of zero charge (pzc), in which the electrode's net surface charge is zero. Either side of the pzc, the net charge at the electrode's surface is either negative (on the left-hand side of pzc in Figure 2 or positive (on the right-hand side of pzc in Figure 2). Theoretically, the maxima of the capacitance curve correspond to the saturation of the Helmholtz layer in the EDL by counterions.[37] From Figure 2b, the pzc for $[C_4mpyr][NTf_2]$ on a gold electrode is reached at ∼-400 mV vs $AgIAg^+$, whereas the maximum capacitance is located at ∼−1500 mV for a negatively charged electrode and between +500 mV and +1200 mV for a positively charged electrode.

As described above, the NR measurements were conducted at three different applied potentials: on the left-hand side of the pzc (at point A in Figure 2b), close to the pzc (point B), and on the right-hand side of the pzc (point C). These three points are located well within the electrochemical window of $[C_4mpyr]$-$[NTf_2]$ (Figure 2a) and chosen to avoid decomposition of the RTIL on gold, which is expected at ∼-2400 mV vs $AgIAg^+$.[56,57] The measured and fitted NR data are plotted as functions of the momentum transfer (Q) in Figure 3.

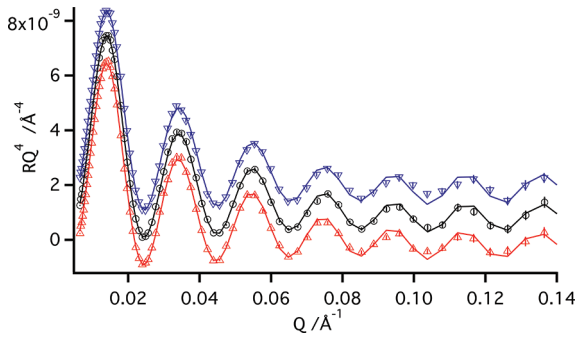

Figure 3. NR curves for ultrahigh purity $[C_4mpyr][NTf_2]$ on a gold electrode at points A (∇, −1595 mV), B (○, −895 mV), and C (Δ, +905 mV), as indicated in Figure 2b. The dots are the measured reflectivity data, whereas the solid lines are the fitted data (using scenario ii). The NR curves at point A and C are offset vertically by plus and minus one unit scale on the ordinate. All experimental uncertainties reported in this paper represent 1 standard deviation.

Subtle, but clear, differences between the three NR curves were observed. To highlight these subtle changes, the NR data for points A and C are plotted on an expanded scale (RQ^4) in Figure 4b, alongside a theoretical NR curve for the situation where there is no excess or segregation of ions at the interface (i.e., equimolar quantities of $[C_4mpyr]^+$ and $[NTf_2]^-$). In addition, Figure 4a shows an 'asymmetry' plot of the difference of the two data sets divided by the sum, $(A - C)/(A + C)$. Such

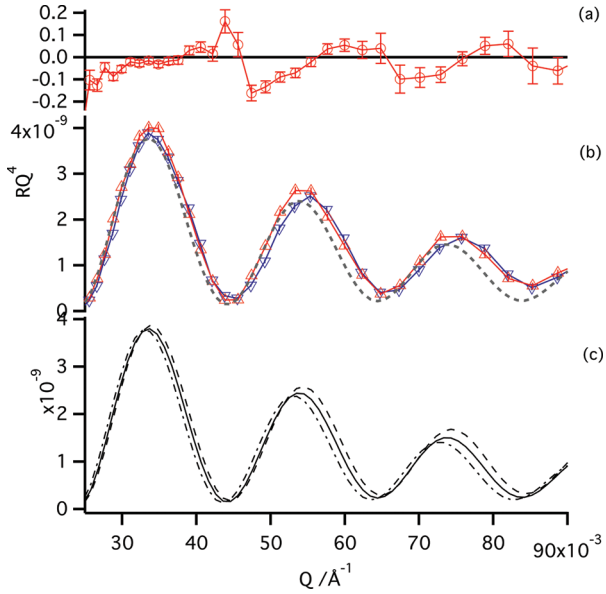

Figure 4. (a) An asymmetry plot that highlights differences between data set A and C. This is obtained by the relationship $(A - C)/(A + C)$, with propagation of errors. (b) Zoom-in view of the measured NR data for data set A (∇) and data set C (Δ), together with the theoretical reflectivity for no excess of either ion. (c) Theoretical NR curves for the cases where there is an excess of either $[C_4mpyr]^+$ (dashed) or $[NTf_2]^-$ (dash-dot) at the interface, and where there is no excess of ions (continuous). All lines are guides to the eye.

plots are regularly used in polarized neutron reflectometry to highlight the differences between two data sets.[58] The presence of oscillations in this asymmetry plot, outside the error bars of the measurement indicates a systematic change in periodicity of the fringes—if no effect was observed then this asymmetry plot would show randomized equi-distribution of points either side of the abscissa across the entire plot region. These changes were also observed in repeat measurements on a different wafer (where the application of applied potential was in reverse order). The data in Figure 4b shows that the Kiessig fringes shift to the right as the applied potential becomes more negative. This is due to an increasing surface excess of $[C_4mpyr]^+$, as illustrated by the three theoretical NR curves shown in Figure 4c. These were generated based on a hypothetical interface where there was a local excess (in a single layer of uniform composition) of either $[C_4mpyr]^+$ or $[NTf_2]^-$, or no excess of either ion close to the surface of the gold electrode. It is apparent that, when the interface is dominated by $[C_4mpyr]^+$, the Kiessig fringes shift to higher Q than those observed with no interfacial excess of either ion. This shift can be explained by considering the relative SLDs of the system. Since the cation possesses an SLD which is lower than that of gold and of the bulk IL, it lowers the amount of scattering density adjacent to the surface, making the Au look thinner. Alternatively, when there is an excess of anion at the interface, the corresponding Kiessig fringes would shift to lower Q values (the anion has an SLD greater than that of the bulk IL and would increase the amount of scattering density at the Au/IL surface, making the Au look thicker). This qualitative analysis therefore indicates that there is a surface excess of cation at *all* surface potentials, although the amount does change as the electrode becomes more positive.

dx.doi.org/10.1021/la3005757 | *Langmuir* 2012, 28, 7374−7381

Table 2. List of Parameters Used to Fit the NR Data in Figure 3 at Points A, B, and C, Using the Volume Fraction Profiles Created by Eq 1

	F	t (Å)	λ (Å)	l (Å)	χ^2	$\sigma_{[C_4mpyr]^+}$(10^{-6} mol.m^{-2})
A						
i	0.5				18.4	0
ii	1.00 ± 0.00	9.0 ± 0.2			2.3	2.81 ± 0.06
iii	1.00 ± 0.00	0	111.4 ± 11.6	10.9 ± 0.7	2.6	2.41 ± 0.06
iv	0.98 ± 0.02	8.8 ± 0.5	16.5 ± 4.4	20.5 ± 1.0	2.2	2.70 ± 0.10
B						
i	0.5				5.8	0
ii	0.99 ± 0.03	8.4 ± 0.5			1.5	2.57 ± 0.07
iii	1.00 ± 0.00	0	167.8 ± 31.4	8.2 ± 0.5	1.6	2.29 ± 0.06
iv	0.89 ± 0.06	9.9 ± 1.4	4.9 ± 3.4	19.1 ± 4.8	1.4	2.35 ± 0.15
C						
i	0.5				12.4	0
ii	0.63 ± 0.02	24.3 ± 3.3			2.0	1.93 ± 0.08
iii	0.76 ± 0.02	0	199.9 ± 0.2	13.9 ± 1.2	2.0	1.89 ± 0.09
iv	0.61 ± 0.02	27.0 ± 2.5	3.6 ± 4.2	16.9 ± 2.7	1.9	1.83 ± 0.17

This qualitative analysis can be understood in more detail by closer examination of the modeling. Several different scenarios can be employed by varying parameters in eq 1:

(i) No surface excess of either ion is present (F = 0.5).
(ii) There is only a layer of constant composition (thickness t) at the interface, with no oscillatory layering (small l) (a "one box model").
(iii) There is only oscillatory layering of ions at the surface (t = 0).
(iv) There is a layer of constant composition and oscillatory layering at the surface.

The parameters from each of these types of fit, for data sets A/B/C, are shown in Table 2.

The excess of $[C_4mpyr]^+$ at the interface ($\sigma_{[C4mpyr]^+}$) was approximated by integrating eq 1 between $0 < z < \infty$, subtracting the amount due to the bulk amount of cation, and dividing by the molecular volume. For case ii, this is simply expressed as

$$\sigma_{[C_4mpyr]^+} = \frac{1}{v_{[C_4mpyr]^+}} t(F - 0.5)$$

where $v_{[C_4mpyr]^+}$ and F are the molar volume and mole fraction of $[C_4mpyr]^+$, respectively. The molar volume of ions used here are $v_{[C_4mpyr]^+} = 1.59 \times 10^{-4}$ m^3/mol and $v_{[NTf_2]^-} = 1.44 \times 10^{-4}$ m^3/mol (molar volume = N_aV_m, where N_a is Avogadro's constant and V_m is the molecular volume of the cation, 263.4 Å^3, or anion, 239.6 Å^3). Note that the molar volume of ions at the interface is assumed to be the same as those in the bulk. This implies that the effect of electrostriction, which is the compression of ions at the interface due to a high electrostatic field, is not taken into account. Further studies are needed to determine accurately the extent of the electrostriction effect. One of the determining factors in electrostriction is the polarizability of ions at the interface. For aqueous electrolytes, ion polarizability is known to decrease in high electrostatic fields.[59] However, the existence of a similar effect in RTILs is still unclear.[37,60]

It is immediately obvious from the χ^2 values that there must be segregation of ions at the surface because case i is a very bad fit.

The remaining cases all describe the data extremely well, with low χ^2 values. Cases ii–iv all have similar surface excesses, $\sigma_{[C_4mpyr]^+}$. Cases ii and iv both have an initial layer of uniform composition adjacent to the electrode surface, with this initial layer providing the majority of the surface excess. In case iv, the parameters controlling the exponential damped cosine wave have relatively high uncertainty, for points A, B and C. The wavelength of the cosine term is also smaller than the typical ion size (you would expect the wavelength to be approximately the sum of the ion sizes) for points B and C, but is more physically reasonable for sample A. However, as mentioned above the oscillatory part provides a relatively small contribution to the surface excess of cation. In comparison to cases ii and iv, case iii does not possess the uniform layer adjacent to the electrode, only the oscillatory part. From inspection of the wavelength and decay length of the wave it is obvious that the wavelength has diverged to a physically unreasonable large value, effectively making the oscillatory part an exponential decay. This exponential decay has the same excess as a layer of uniform composition (case ii, but both fits are of equal quality. It should be noted that attempts were made to constrain the wavelength of the oscillatory part to the size of the ion pair, but poor fits were obtained.

In general, these results indicate that the relatively narrow Q-range of the data limits the sensitivity of NR to detect structural details on an Angstrom scale, such as alternating layers of ions. This means we cannot distinguish which of cases ii, iii, or iv is "correct". Nevertheless, the NR data still provides us with solid information on the excess amount of ions at the interface and the overall interfacial thickness (t). Indeed, the decay length for case iii (which is effectively an exponential) is reasonably similar to the thickness of the uniform layer in case ii. From this point on the discussion will use values obtained from scenario ii.

Table 2 shows that $\sigma_{[C_4mpyr]^+}$ decreases as the electrode potential becomes more positive, i.e., from 2.81×10^{-6} mol/m^2 (1.69 $[C_4mpyr]^+$ molecules per nm^2) at point A to 1.93×10^{-6} mol/m^2 (1.16 $[C_4mpyr]^+$ molecules per nm^2) at point C. Surprisingly, there is still a net excess of $[C_4mpyr]^+$ at point C, where the electrode is positively charged. At point A the interface is occupied only by $[C_4mpyr]^+$. The average thickness of this interface (9.0 Å) is similar to the characteristic length of

dx.doi.org/10.1021/la3005757 | Langmuir 2012, 28, 7374–7381

$[C_4mpyr]^+$. This suggests that the interface is formed either by a monolayer of $[C_4mpyr]^+$ where the cations are oriented perpendicularly to the electrode's surface, or by a stack of $[C_4mpyr]^+$ where the heterocylic ring of $[C_4mpyr]^+$ is oriented parallel to the electrode's surface in a similar fashion to that observed for imidazolium-based cations at negatively charged platinum, silver, or copper electrodes.[39−42]

At point B (close to the pzc), the interface is still entirely composed of $[C_4mpyr]^+$. However, it is slightly thinner than that at point A. A thicker interface at point A is expected since the Helmholtz layer of the interface is supposedly saturated by cations.[37] The thickness of the interface at point B (8.4 ± 0.5 Å) is similar to the thickness of the first layer of $[C_4mpyr]$-$[NTf_2]$ on a gold surface measured by AFM at a comparable open circuit potential.[61] The total thickness of the interface measured by AFM is ∼38 Å, i.e., almost five times the interfacial thickness found in our study. There are several possible explanations for this discrepancy: (i) each layer probed by AFM does not necessarily correspond to a local excess of cation or anion. Instead, it could be a self-assembled layer made of an equal number of cations and anions, as found in the bulk; (ii) the crystalline phase of the gold electrode used in both experiments were different. In this study, we used a polycrystalline gold electrode where the Au(111) was the dominant orientational plane, whereas the AFM measurement was conducted on a monocrystalline Au(111) surface; (iii) the restricted Q range of the measurement means that NR is only sensitive to the average behavior of the scattering length density profile from the electrode toward the bulk liquid, where fluctuations in scattering length density are largest. This means that the furthest extent of the interface, where the molar concentrations approach that of the bulk, would not be detected by NR, but would be by AFM.

At point C, the interface consists of 63% mole fraction of $[C_4mpyr]^+$ and 37% $[NTf_2]^-$, considerably less than at points A and B. On the other hand the thickness of the uniform layer (24.3 Å) is larger than that at point A and B. This indicates that the layer is more diffuse. However, the net excess of $[C_4mpyr]^+$ at the interface at point C is unexpected since an excess of $[NTf_2]^-$ was anticipated in order to balance the positive charge on the electrode. One of the possible factors which can cause the excess of cations is the specific (nonelectrostatic) adsorption of $[C_4mpyr]^+$ on the gold electrode. A strong affinity of cations or anions of RTILs toward solid surfaces has been previously reported in the literature.[62,63] The absence of any solvating molecules in RTILs leads to strong specific adsorption because there is no steric barrier preventing ions from physically or chemically interacting with the electrode's surface. In aqueous solutions, the specific adsorption is typically dominant within approximately 10 k_BT (250 mV) from the pzc.[64−66] In RTILs, any changes in the EDL structure caused by specific adsorption would be significant over a wider range of potential values due to the absence of (co)solvating media. This may explain the excess of $[C_4mpyr]^+$ at the interface at point C, which is located ∼1300 mV to the right-hand side of pzc.

A better understanding of the extent of the specific adsorption effect in RTILs is important. If this effect remains prominent at high potential fields, the corresponding EDL structures would be strongly determined not only by long-range electrostatic forces, but also by relatively short-range effects originated from the specific affinity of ions toward the electrode's surface. It would also be intriguing to find out the extent to which the specific adsorption effect is reduced by the presence of cosolvents, such as water, in RTILs. The impact of specific adsorption on the interfacial structure of pure RTILs and RTIL−water mixtures is the current focus of our research. Results of this study will be reported in the near future.

■ CONCLUSIONS

The EDL structure of the RTIL $[C_4mpyr][NTf_2]$ at a gold-liquid interface was studied as a function of the applied electrode potential using NR. The corresponding electrochemical window and pzc were determined from the cyclic voltammogram and differential capacitance curves, respectively. A series of NR data was collected at three applied potential values, viz., at a potential more negative than the pzc, close to the pzc, and at a potential more positive than the pzc. The NR data were fitted using a space filling model consisting of a layer of uniform mole fraction of cation adjacent to the electrode, followed by an exponentially damped cosine wave. Clear, but subtle differences between all the NR curves were observed. Although the limited Q range prevented observation of cation/anion layering, detailed analysis of the fitted reflectivity data indicate a thin, compact layer almost entirely consisting of $[C_4mpyr]^+$ at the most negative potentials, with this layer becoming more diffuse at positive applied potential. As expected, the excess amount of $[C_4mpyr]^+$ at the interface decreases as the electrode becomes positive. However, a surface excess of $[C_4mpyr]^+$ was still found at a positively charged electrode, which we ascribe to the specific adsorption of $[C_4mpyr]^+$ at the gold electrode.

■ ASSOCIATED CONTENT

Ⓢ Supporting Information

Computer code for modeling this data and neutron reflectometry data sets and a schematic of the electrochemical cell used for the measurements. This material is available free of charge via the Internet at http://pubs.acs.org/.

■ AUTHOR INFORMATION

Corresponding Author

*E-mail: Andrew.Nelson@ansto.gov.au.

Notes

The authors declare no competing financial interest.

■ ACKNOWLEDGMENTS

We thank Dr. B. Follink, Dr. G.A. Snook, Dr. NAS Webster (CSIRO); Dr. R. Knott (ANSTO); Dr. N. Maliszewskyj and Dr. A. Jackson (NIST) for their support in this work. Y. Lauw would like to acknowledge financial support from the Access to Major Research Facilities Programme (ref 08/09-N-22), which is a component of the International Science Linkages Programme established under the Australian Government's innovation statement, "Backing Australia's Ability". Some preliminary NR measurements were conducted at the NIST Center for Neutron Research using the NG7 reflectometer, under Proposal Number R23-13. The main NR data were collected using Platypus instrument at ANSTO, under Proposal ID P1071 and IC831.

■ REFERENCES

(1) Welton, T. Room-temperature ionic liquids. Solvents for synthesis and catalysis. *Chem. Rev.* **1999**, *99*, 2071.

(2) *Ionic Liquids in Synthesis*; Wiley-VCH: Weinheim, Germany, 2003.

(3) Zhang, S.; Sun, N.; He, X.; Lu, X.; Zhang, X. Physical properties of ionic liquids: Database and evaluation. *J. Phys. Chem. Ref. Data* **2006**, *35*, 1475.
(4) Endres, F.; Abedin, S. Z. E. Air and water stable ionic liquids in physical chemistry. *Phys. Chem. Chem. Phys.* **2006**, *8*, 2101.
(5) Rogers, R. D. Materials science - Reflections on ionic liquids. *Nature* **2007**, *447*, 917.
(6) Endres, F. Ionic Liquids: Solvents for the Electrodeposition of Metals and Semiconductors. *ChemPhysChem* **2002**, *3*, 144.
(7) Sato, T.; Masuda, G.; Takagi, K. Electrochemical properties of novel ionic liquids for electric double layer capacitor applications. *Electrochim. Acta* **2004**, *49*, 3603.
(8) *Electrochemical aspects of ionic liquids*; John Wiley & Sons, Inc.: New York, 2005.
(9) Moustafa, E. M.; Abedin, S. Z. E.; Shkurankov, A.; Zchippang, E.; Saad, A. Y.; Bund, A.; Endres, F. Electrodeposition of al in 1-butyl-1-methylpyrrolidinium bis(trifluoromethylsulfonyl)amide and 1-ethyl-3-methylimidazolium bis(trifluoromethylsulfonyl)amide ionic liquids: In situ STM and EQCM studies. *J. Phys. Chem. B* **2007**, *111*, 4693.
(10) *Electrodeposition from Ionic Liquids*. Wiley-VCH: Weinheim, Germany, 2008.
(11) Simon, P.; Gogotsi, Y. Materials for electrochemical capacitors. *Nat. Mater.* **2008**, *7*, 845.
(12) Arbizzani, C.; Biso, M.; Cericola, D.; Lazzari, M.; Soavi, F.; Mastragostino, M. Safe, high-energy supercapacitors based on solvent-free ionic liquid electrolytes. *J. Power Sources* **2008**, *185*, 1575.
(13) Armand, M.; Endres, F.; MacFarlane, D.; Ohno, H.; Scrosati, B. Ionic-liquid materials for the electrochemical challenges of the future. *Nat. Mater.* **2009**, *8*, 621.
(14) Kroll, W. J. The Production of Ductile Titanium. *Transactions of the Electrochemical Society* **1940**, *78*, 35.
(15) *Handbook of Extractive Metallurgy*. Wiley-VCH: Weinheim, Germany, 1997.
(16) Katayama, Y.; Fukui, R.; Miura, T. Electrodeposition of cobalt from an imide-type room-temperature ionic liquid. *J. Electrochem. Soc.* **2007**, *154*, D534.
(17) Vaughan, J.; Tu, J.; Dreisinger, D. Ionic liquid electro-deposition of reactive metals. *Trans.—Inst. Min. Metall., Sect.C* **2008**, *117*, 113.
(18) Horn, R. G.; Evans, D. F.; Ninham, B. W. Double-layer and solvation forces measured in a molten-salt and its mixtures with water. *J. Phys. Chem.* **1988**, *92*, 3531.
(19) Carmichael, A. J.; Hardacre, C.; Holbrey, J. D.; Nieuwenhuyzen, M.; Seddon, K. R. Molecular layering and local order in thin films of 1-alkyl-3-methylimidazolium ionic liquids using X-ray reflectivity. *Mol. Phys.* **2001**, *99*, 795.
(20) Bowers, J.; Vergara-Gutierrez, M. C. Surface ordering of amphiphilic ionic liquids. *Langmuir* **2004**, *20*, 309.
(21) Sloutskin, E.; Ocko, B. M.; Tamam, L.; Kuzmenko, I.; Gog, T.; Deutsch, M. Surface layering in ionic liquids: An X-ray reflectivity study. *J. Am. Chem. Soc.* **2005**, *127*, 7796.
(22) Atkin, R.; Warr, G. G. Structure in confined room-temperature ionic liquids. *J. Phys. Chem. C* **2007**, *111*, 5162.
(23) Mezger, M.; Schroder, H.; Reichert, H.; Schramm, S.; Okasinski, J. S.; Schoder, S.; Honkimaki, V.; Deutsch, M.; Ocko, B. M.; Ralston, J.; Rohwerder, M.; Stratmann, M.; Dosch, H. Molecular layering of fluorinated ionic liquids at a charged sapphire (0001). *Surf. Sci.* **2008**, *322*, 424.
(24) Su, Y. Z.; Fu, Y. C.; Yan, J. W.; Chen, Z. B.; Mao, B. W. Double Layer of Au(100)/Ionic Liquid Interface and Its Stability in Imidazolium-Based Ionic Liquids. *Angew. Chem., Int. Ed.* **2009**, *48*, 5148.
(25) Lauw, Y.; Horne, M. D.; Rodopoulos, T.; Webster, N. A. S.; Minofar, B.; Nelson, A. X-Ray reflectometry studies on the effect of water on the surface structure of [C(4)mpyr][NTf(2)] ionic liquid. *Phys. Chem. Chem. Phys.* **2009**, *11*, 11507.
(26) Mezger, M. S., S.; Schröder, H.; Reichert, H.; Deutsch, M.; De Souza, E.; Okasinski, J. S.; Ocko, B. M.; Honkimäki, V.; Dosch, M. Layering of $[BMIM]^+$-based ionic liquids at a charged sapphire interface. *J. Chem. Phys.* **2009**, 131.
(27) Bikerman, J. J. Structure and capacity of electrical double layer. *Philos. Mag.* **1942**, *33*, 384.
(28) Freise, V. *Z. Elektrochem.* **1952**, *56*, 822.
(29) Marcus, R. A. On the Theory of Oxidation-Reduction Reactions Involving Electron Transfer. I. *J. Chem. Phys.* **1956**, *24*, 966.
(30) Marcus, R. A. Electrostatic Free Energy and Other Properties of States Having Nonequilibrium Polarization. I. *J. Chem. Phys.* **1956**, *24*, 979.
(31) Kilic, M. S.; Bazant, M. Z.; Ajdari, A. Steric effects in the dynamics of electrolytes at large applied voltages. I. Double-layer charging. *Phys. Rev. E.* **2007**, *75*, 021502.
(32) Kornyshev, A. A. Double-layer in ionic liquids: Paradigm change? *J. Phys. Chem. B* **2007**, *111*, 5545.
(33) Oldham, K. B. A Gouy-Chapman-Stern model of the double layer at a (metal)/(ionic liquid) interface. *J. Electroanal. Chem.* **2008**, *613*, 131.
(34) Reed, S. K.; Madden, P. A.; Papadopoulos, A. Electrochemical charge transfer at a metallic electrode: A simulation study. *J. Chem. Phys.* **2008**, *128*, 124701.
(35) Bazant, M. Z.; Kilic, M. S.; Storey, B. D.; Ajdari, A. Nonlinear electrokinetics at large voltages. *New J. Phys.* **2009**, *11*, 075016.
(36) Lockett, V.; Sedev, R.; Ralston, J.; Horne, M. D.; Rodopoulos, T. Differential capacitance of the electrical double layer in imidazolium-based ionic liquids: Influence of potential, cation size, and temperature. *J. Phys. Chem. C* **2008**, *112*, 7486.
(37) Lauw, Y.; Horne, M.; Rodopoulos, T.; Leermakers, F. A. M. Room-Temperature Ionic Liquids: Excluded Volume and Ion Polarizability Effects in the Electrical Double-Layer Structure and Capacitance. *Phys. Rev. Lett.* **2009**, *103*, 117801.
(38) Abedin, S. Z. E.; Moustafa, E. M.; Hempelmann, R.; Natter, H.; Endres, F. Electrodeposition of nano- and microcrystalline aluminium in three different air and water stable ionic liquids. *ChemPhysChem* **2006**, *7*, 1535−1543.
(39) Rivera-Rubero, S.; Baldelli, S. Surface spectroscopy of room-temperature ionic liquids on a platinum electrode: A sum frequency generation study. *J. Phys. Chem. B* **2004**, *108*, 15133.
(40) Santos, V. O.; Alves, M. B.; Carvalho, M. S.; Suarez, P. A. Z.; Rubim, J. C. Surface-enhanced Raman scattering at the silver electrode/ionic liquid (BMIPF6) interface. *J. Phys. Chem. B* **2006**, *110*, 20379.
(41) Baldelli, S. Surface structure at the ionic liquid-electrified metal interface. *Acc. Chem. Res.* **2008**, *41*, 421.
(42) Yuan, Y. X.; Niu, T. C.; Xu, M. M.; Yao, J. L.; Gu, R. A. Probing the adsorption of methylimidazole at ionic liquids/Cu electrode interface by surface-enhanced Raman scattering spectroscopy. *J. Raman Spectrosc.* **2010**, *41*, 516.
(43) MacFarlane, D.; Meakin, P.; Sun, J.; Amini, N.; Forsyth, M. Pyrrolidinium imides: A new family of molten salts and conductive plastic crystal phases. *J. Phys. Chem. B* **1999**, *103*, 4164.
(44) The electrochemical and physicochemical performances of RTILs are often influenced by their water content. For example, [NTf2]-based RTILs are hygroscopic and trace amounts of water would reduce the electrochemical window of these RTILs.
(45) Lauw, Y.; Rodopoulos, T.; Gross, M.; Nelson, A.; Gardner, R.; Horne, M. D. Electrochemical cell for neutron reflectometry studies of the structure of ionic liquids at electrified interface. *Rev. Sci. Instrum.* **2010**, *81*, 074101.
(46) Ozonolysis removes organic contaminants from the surface of the gold. X-ray reflectometry patterns measured from these surfaces before and after ozonolysis are invariant, indicating that the surface is not roughened or oxidised.
(47) Commercial materials, instruments and equipment are identified in this paper in order to specify the experimental procedure as completely as possible. In no case does such identification imply a recommendation or endorsement by the National Institute of Standards and Technology, nor does it imply that the materials, instruments, or equipment identified are necessarily best available for the purpose.

(48) Sears, V. F. Neutron scattering lengths and cross sections. *Neutron News* **1992**, 26−37.
(49) Krossing, I.; Slattery, J. M.; Daguenet, C.; Dyson, P. J.; Oleinikova, A.; Weingartner, H. Why are ionic liquids liquid? A simple explanation based on lattice and solvation energies. *J. Amer. Chem. Soc.* **2006**, *128*, 13427.
(50) Kobrak, M. N. The relationship between solvent polarity and molar volume in room-temperature ionic liquids. *Green Chem.* **2008**, *10*, 80.
(51) James, M.; Nelson, A.; Holt, S. A.; Saerbeck, T.; Hamilton, W. A.; Klose, F. The multipurpose time-of-flight neutron reflectometer "Platypus" at Australia's OPAL reactor. *Nuclear Instrum. Methods Phys. Res. A* **2011**, *632*, 112−123.
(52) Nelson, A. Motofit - integrating neutron reflectometry acquisition, reduction and analysis into one, easy to use, package. *J. Phys., Conf. Ser.* **2010**, *251*, 012094.
(53) Lockett, V.; Horne, M.; Sedev, R.; Rodopoulos, T.; Ralston, J. Orientation and mutual location of ions at the surface of ionic liquids. *Phys. Chem. Chem. Phys.* **2010**, *12*, 12499−12512.
(54) Nelson, A. Co-refinement of multiple contrast neutron/X-ray reflectivity data using MOTOFIT. *J. Appl. Crystallogr.* **2006**, *39*, 273−276.
(55) Nevot, F.; Croce, P. Caractérisation des surfaces par réflexion rasante de rayons X. Application à l'étude du polissage de quelques verres silicates. *Rev. Phys. Appl.* **1980**, *15*, 761.
(56) Howlett, P. C.; Izgorodina, E.; Forsyth, M.; MacFarlane, D. Electrochemistry at negative potentials in bis-(trifluoromethanesulfonyl)amide ionic liquids. *Z. Phys. Chem.* **2006**, *220*, 1483.
(57) Endres, F.; Abedin, S. Z. E.; Borisenko, N. Probing lithium and alumina impurities in air- and water stable ionic liquids by cyclic voltammetry and in situ scanning tunneling microscopy. *Z. Phys. Chem.* **2006**, *220*, 1377.
(58) Saoudi, M.; Fritzsche, H.; Nieuwenhuys, G. J.; Hesselberth, M. B. S. Size Effect in the Spin Glass Magnetization of Thin AuFe Films as Studied by Polarized Neutron Reflectometry. *Phys. Rev. Lett.* **2008**, *100* (5), 057204.
(59) Teschke, O.; Ceotto, G.; de Souza, E. F. Interfacial aqueous solutions dielectric constant measurements using atomic force microscopy. *Chem. Phys. Lett.* **2000**, *326*, 328.
(60) Kobrak, M. N.; Li, H. Electrostatic interactions in ionic liquids: the dangers of dipole and dielectric descriptions. *Phys. Chem. Chem. Phys.* **2010**, *12*, 1922.
(61) Atkin, R.; Abedin, S. Z. E.; Hayes, R.; Gasparotto, L. H. S.; Borisenko, N.; Endres, F. AFM and STM Studies on the Surface Interaction of [BMP]TFSA and (EMIm]TFSA Ionic Liquids with Au(111). *J. Phys. Chem. C* **2009**, *113*, 13266.
(62) Gale, R. J.; Osteryoung, R. A. The electrical double layer at mercury in room temperature aluminum chloride: 1-butylpyridinium chloride ionic liquids. *Electrochim. Acta* **1980**, *25*, 1527.
(63) Aliaga, C.; Baldelli, S. Sum frequency generation spectroscopy and double-layer capacitance studies of the 1-butyl-3-methylimidazolium dicyanamide-platinum interface. *J. Phys. Chem. B* **2006**, *110*, 18481.
(64) Parsons, R. The specific adsorption of ions at the metal-electrolyte interphase. *Trans. Faraday Soc.* **1955**, *51*, 1518.
(65) Nikitas, P. A new approach to development of ionic isotherms of specific adsorption in the electrical double-layer. *J. Phys. Chem.* **1994**, *98*, 6577.
(66) Lamperski, S. Molecular model for anion adsorption from electrolyte of constant ionic strength. *J. Electroanal. Chem.* **1997**, *437*, 225.